

A preliminary study of the weathering mechanism of fossilized Cretaceous *Hamipterus* bones

Ying LI^{1,2†}, Wugan LUO^{1,2†}, Yimin YANG^{1,2}, Shunxing JIANG^{1,3} & Xiaolin WANG^{1,3,4*}¹ Key Laboratory of Vertebrate Evolution and Human Origins of Chinese Academy of Sciences, Institute of Vertebrate Paleontology and Paleoanthropology, Chinese Academy of Sciences, Beijing 100044, China;² Department of Archaeology and Anthropology, University of Chinese Academy of Sciences, Beijing 100049, China;³ CAS Center for Excellence in Life and Paleoenvironment, Beijing 100044, China;⁴ College of Earth and Planetary Sciences, University of Chinese Academy of Sciences, Beijing 100049, China

Received April 20, 2020; revised October 21, 2020; accepted November 10, 2020; published online January 20, 2021

Abstract The discovery of *Hamipterus tianshanensis* had important scientific significance because three-dimensional preserved fossils can provide unique information about the reproduction, development, and evolution of pterosaurs. However, the pterosaur fossils exhibited violent weathering, including noticeable cracking and spalling, since the preservation environment changed dramatically after excavation, which severely influenced the preservation of these fossils and the scientific research conducted on them. To determine the weathering mechanism of these fossil bones, the samples were analyzed using X-ray fluorescence (XRF), Fourier transform infrared spectroscopy (FTIR), X-ray diffraction (XRD), scanning electron microscopy and energy dispersive spectrometry (SEM-EDS). The results indicate that calcite is the main mineral in the hollow bones, but it is mixed with a small amount of other minerals, such as quartz, feldspar, and other debris particles. Moreover, the main component of the pterosaur bones is hydroxyapatite, and carbonate has substituted for some of the phosphate (B-type carbonated apatite) in the fossil bones. A small amount of calcite and manganese oxides has precipitated in the vascular canals. The phosphate crystallinity index (PCI) is 4.17. These results indicate that the fossils have undergone severe diagenesis. Apart from these alterations, the fossil bones have high contents of anions and cations such as Cl^- , NO_3^- , SO_4^{2-} , Na^+ , and Ca^{2+} , and the total content of soluble salts is $35584.41 \mu\text{g g}^{-1}$. Based on these results, it is inferred that the weathering mechanism of the fossil bones is as follows. First, the fragile hollow bones cracked easily because of the enormous thermal stress caused by the dramatic temperature changes in the Gobi Desert and the differences in the thermal expansion coefficients (TEC) of the surrounding rocks, the fossil bones, and the different fillers. Second, a large amount of stress is generated by salt crystallization when the temperature and humidity change, and the pterosaur fossils will be damaged when the crystallization pressure exceeds the tensile strength of the fossils. These results suggest that the preservation of pterosaur fossils requires suitable desalination and consolidation conditions. Moreover, they should be preserved in a constant temperature and humidity environment.

Keywords *Hamipterus*, fossil weathering, hydroxyapatite, coefficient of thermal expansion, Xinjiang

Citation: Li Y, Luo W, Yang Y, Jiang S, Wang X. 2021. A preliminary study of the weathering mechanism of fossilized Cretaceous *Hamipterus* bones. Science China Earth Sciences, 64(3): 458–469, <https://doi.org/10.1007/s11430-020-9702-8>

1. Introduction

Paleontological fossils, which are precious nonrenewable

natural relics, are the key to understanding the lives of ancient organisms on Earth. Among the few pterosaur fossil localities around the world, the Turpan-Hami Basin, Xinjiang, China, is a unique site because it is not only the largest and the richest source of pterosaur bones in the world but

* Corresponding author (email: wangxiaolin@ivpp.ac.cn)

† These authors contributed equally to this work.

also the only site containing preserved three-dimensional (3D) male and female skulls, eggs, and embryos together (Wang et al., 2018). The pterosaur (*Hamipterus tianshanensis*) preserved in the Hami Basin shed light on the reproductive strategy, ontogeny, behavior, and ecology of pterosaurs (Martill, 2014; Wang et al., 2014, 2017; Deeming, 2017). However, these precious fossils experienced weathering after their excavation and transportation from Xinjiang to Beijing. The degradation, such as the powdering and disintegration of the rocks surrounding the fossils and spalling of the fossil bones, has severely affected the preservation, exhibition, and scientific research of these fossils.

Although the weathering resistance of most fossil bones is improved after fossilization, some fossils still undergo weathering phenomena such as cracking and spalling. Several studies have been conducted on the preservation of weathered fossils. For dinosaur fossils found in China, Deng et al. (2010b) used Fourier transform infrared spectroscopy (FTIR), X-ray diffraction (XRD), and other chemical analysis methods to determine the compositions of the fossils and their matrix, and then, they used nano SiO₂ hybrid emulsion to consolidate the fossils (Deng et al., 2010a). For a human mandible from Atapuerca (Spain), López-Polín et al. (2008) used computer tomography (CT) scans and other techniques to complete the diagnostic examination before physical intervention, and then, they used the reagents such as demineralized water and alcohol solution (1:1) to clean the fossils and used B72 to rejoin the fossil fragments. For elephant and ivory fossils, researchers have found that the loss of collagen and the deposition of pyrite and goethite are the main factors causing fossil deterioration. After identifying the weathering mechanism, they recommended the use of nano-hydroxyapatite to consolidate fossils and to preserve the fossils in an appropriate environment during storage and exhibition (Turner-Walker, 1998; Wang et al., 2007; Liu, 2014). Whether these conservation methods will negatively interfere with subsequent studies is of great concern. Therefore, several researches have assessed the possible effects of cleaning and consolidation techniques on isotopic and DNA studies of bone tissue (Howie, 1984; López-Polín, 2012; Mallouchou et al., 2019).

As can be seen from these previous studies, understanding the weathering mechanisms is an important initial step in conservation intervention. However, few studies have focused on investigating the weathering mechanisms of fossils, and only a few such studies have been conducted on dinosaur fossils and Pleistocene mammal fossils (Turner-Walker, 1998; Zhang et al., 2019). Until now, far too little attention has been paid to the conservation of pterosaur fossils, the bones of which are thin and hollow. While some researches have discussed the weathering mechanism of pterosaur fossil matrices (Li et al., 2019) and consolidating materials (Peng et al., 2020), the weathering mechanism of pterosaur bones

has not been discussed in detail. For the pterosaur (*Hamipterus Tianshanensis*) fossils found in Xinjiang, the dry and extremely alkaline and saline environment is the main factor that has caused the deterioration of many relics (Liang, 2009). Determining whether or not the deterioration of the fossil bones is related to this extreme environment requires a systematic analysis. Understanding the weathering mechanism of pterosaur fossils is of great significance to developing detailed protection plans. Thus, in this study, X-ray fluorescence (XRF), FTIR, XRD, scanning electron microscopy and energy dispersive spectrometry (SEM-EDS), and ion chromatography (IC) were used to investigate the weathering and degradation mechanism of fossil bones and to provide a valuable reference for fossil conservation.

2. Material, methods, and results

2.1 Sample testing

The samples used in this study were collected from Hami, Xinjiang, China, where many pterosaur fossils have been excavated. Nearly all of the fossils were found in the tephrite interlayers in the Lower Cretaceous Tugulu Group, which were formed under fluviolacustrine conditions. The fossil matrix is grayish white medium-to-fine grained sandstone mixed with brown mudstone breccias (Wang et al., 2014). The pterosaur fossils are preserved in large quantities individually and without orientation (Wang et al., 2014). The features of the pterosaur fossils are their thin and hollow bones, which are filled with light colored (Figure 1a) and dark colored sandstone (Figure 1b) and transparent, colorless crystals (Figure 1f). Weathering phenomena such as cracking and spalling are severe (Figures 1c and 1e).

2.2 Methods and results

2.2.1 XRF

The chemical compositions of the samples were determined using a laboratory XRF system (XGT-7000, Horiba). A spot size of 1.2 mm, an operating X-ray tube voltage of 30 kV, a current of 0.15 mA, and a data acquisition time of 100 s were chosen. The results are presented in Table 1.

The XRF results indicate that the fossil bones are characterized by low SiO₂ and Al₂O₃ contents, and high CaO and P₂O₅ contents. The main elements of the fossil bones are Ca and P. The Ca/P ratio (1.16) is significantly lower than that of hydroxyapatite (1.67), which suggests that minor elements likely substitute for Ca in the hydroxyapatite structures during diagenetic processes (Newesely, 1989). Remarkably, the fossil bones contain Na₂O and SO₃, indicating that some soluble salts have been deposited within the bones.

The sandstone-filled matrix is characterized by high SiO₂, Al₂O₃, and CaO contents, and low Na₂O, MgO, and Fe₂O₃

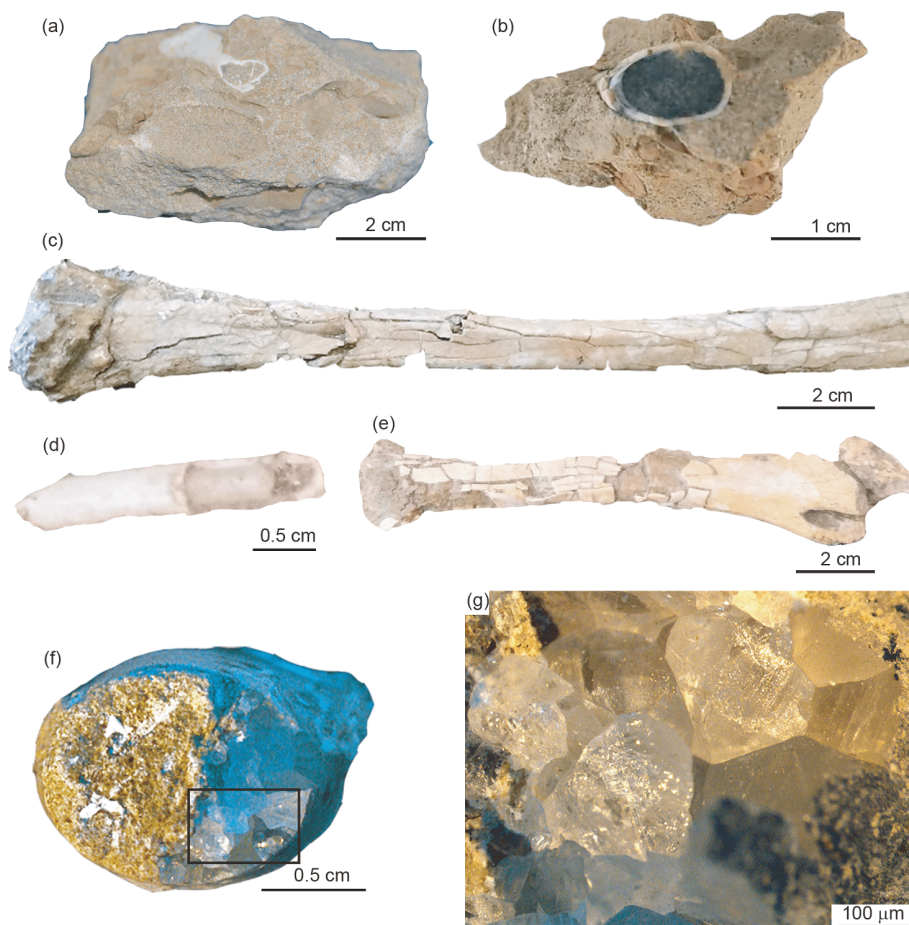


Figure 1 Sample testing of pterosaur fossils. (a) Matrix, fossil bones and light sandstone-filled matrix. (b) Matrix, fossil bones and dark sandstone-filled matrix. (c) Cracked fossil bones. (d) Transparent, colorless crystals filling the hollow bones. (e) Cracking and spalling of pterosaur bones. (f) Cross-section of the filling matrix and colorless crystals partly filling a hollow bone. (g) The magnified image of the interesting part in (f) (black box) and the transparent, colorless crystals.

Table 1 The XRF results for the fossil bones and sandstone-filled matrix (wt%^{a)})

Sample	Na ₂ O	MgO	Al ₂ O ₃	SiO ₂	P ₂ O ₅	SO ₃	Cl	K ₂ O	CaO	TiO ₂	MnO	Fe ₂ O ₃	SrO
YL-B	3.24	6.26	11.71	40	0.13	0.44	–	0.63	22.44	–	12.83	2.06	0.07
YL-W	2.67	2.81	7.86	36.44	0	2.33	–	1.72	41.64	0.4	0.08	4.01	0.03
YL-G	2.71	1.14	1.18	4.61	39.92	1.6	0.03	0.02	46.16	–	–	–	–

a) Throughout this article, YL-B, YL-W, and YL-G refer to the dark sandstone-filled matrix, the light sandstone-filled matrix, and the fossil bones, respectively.

contents. There is no significant difference between the compositions of the dark and light sandstone-filled matrices, except that the dark sandstone-filled matrix has a lower CaO content and a higher MnO content, revealing that the high Mn content mainly contributes to the color of the dark sandstone-filled matrix.

2.2.2 XRD

The X-ray powder diffraction testing of the YL-W, YL-B, and YL-G samples was conducted in the Testing and Analytical Lab at the Xi'an Center of the Chinese Geological Survey. These data were collected using a Rigaku D/max

2500 diffractometer (graphite monochromated, Cu K α radiation, 40 kV, and 200 mA). Before being tested, the samples were crushed using a mortar and pestle and the particles were spread within calibrated recesses on glass slides. The results are shown in Figure 2 and Table 2.

The crystals in the hollow pterosaur bones were scraped out using a scalpel and were ground using a mortar and pestle. The powdered sample was analyzed on XRD (Mini-Flex II; Rigaku, Japan) using Cu K α radiation at 30 kV and 15 mA with a 1.25° divergence slit, a 1.25° anti-scatter slit, and a 0.3 mm receiving slit. The 2 θ scanning range was 15°–70°, with a scanning rate of 3° min⁻¹. The results show that

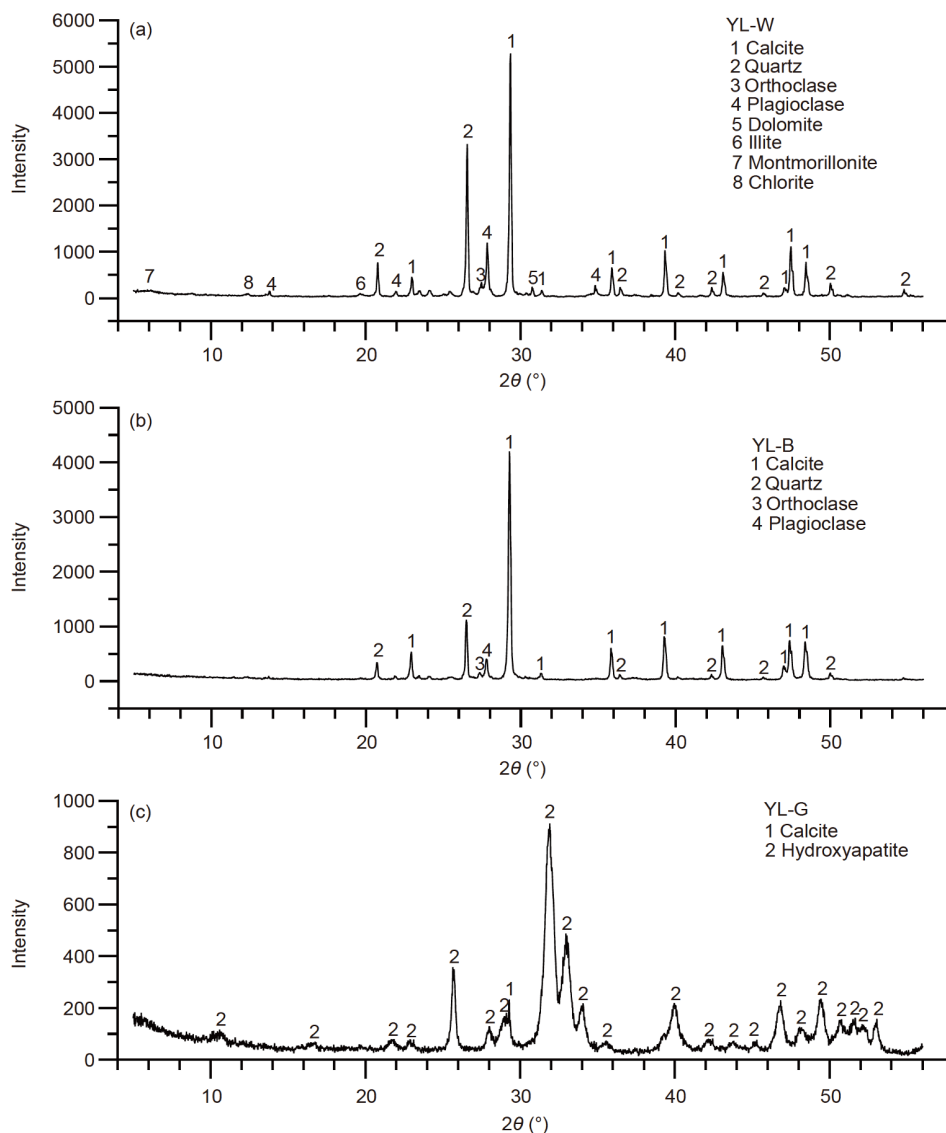


Figure 2 XRD patterns of the samples. (a) The light sandstone-filled matrix; (b) the dark sandstone-filled matrix; and (c) the pterosaur bones.

Table 2 The XRD data (wt%)^{a)}

Samples	YL-W	YL-B	YL-G
Quartz	26.8	15.4	–
Plagioclase	12.7	11.1	–
Orthoclase	4.1	3.8	–
Calcite	45.1	69.7	2
Dolomite	2.3	–	–
Chlorite	2.0	–	–
Illite	3.0	–	–
Montmorillonite	4.0	–	–
Hydroxyapatite	–	–	98

a) The XRD results indicate that the main mineralogical composition of the fossil bones is hydroxyapatite, and they have low calcite content. The sandstone-filled matrix is mainly composed of calcite, with some feldspar and quartz. In addition to these minerals, the light sandstone-filled matrix also contains small amounts of dolomite and clay minerals.

the crystals within the hollow bone are calcite (Figure 3).

In summary, these results show that the main composition of the fossil bones is hydroxyapatite, and they have low calcite content. The sandstone-filled matrix is mainly composed of calcite, with some feldspar, quartz, and clay minerals. The mineral crystals within the hollow bone are calcite.

2.2.3 FTIR

A Pterosaur fossil bone was ground with KBr in an agate mortar at a weight ratio of 1:100 to prepare a tablet. The FTIR spectra were collected using a NICOLET 6700 (Thermo Scientific, USA) spectrometer, within the range of 4000–400 cm^{-1} , at a resolution of 4 cm^{-1} , using 32 scans per spectrum. The data were analyzed using the OMNIC 8.0 software.

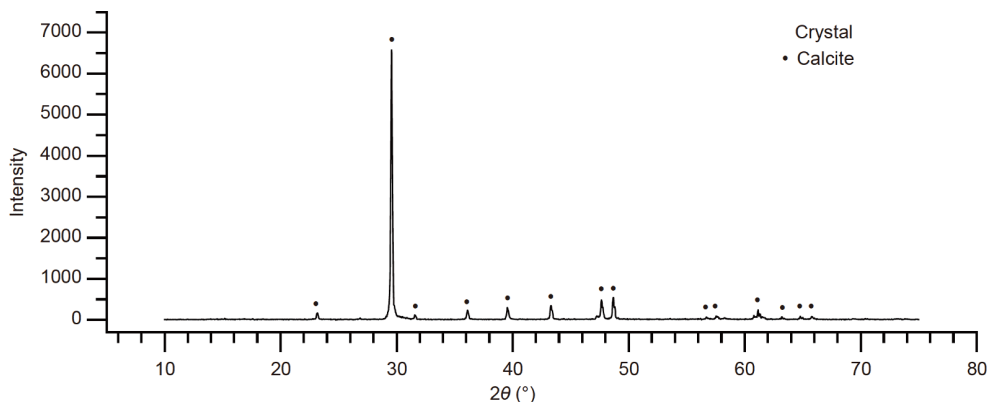


Figure 3 XRD patterns of the crystals within the hollow bone.

The results are shown in [Figure 4](#). The broad bands at 3420 and 1637 cm^{-1} represent the stretching and bending vibrations of the hydroxyl groups, respectively, which shows that the bones contain hydroxyls or adsorbed water. The peaks at 1456 and 1425 cm^{-1} are due to $\nu_3 \text{CO}_3^{2-}$, and the band at 873 cm^{-1} is due to $\nu_2 \text{CO}_3^{2-}$. The strong peak at 1041 cm^{-1} is due to $\nu_3 \text{PO}_4^{3-}$. The bands at 965 and 469 cm^{-1} are due to $\nu_1 \text{PO}_4^{3-}$ and $\nu_2 \text{PO}_4^{3-}$, respectively. The bands at 605 and 570 cm^{-1} are due to $\nu_4 \text{PO}_4^{3-}$ ([Weng and Xu, 2016](#)).

The carbonate ions in the hydroxyapatite can either substitute for the OH^- or PO_4^{3-} , creating A-type and B-type carbonated hydroxyapatite, respectively. The A-type carbonate exhibits bands at about 1545, 1450, and 880 cm^{-1} , while the B-type exhibits bands at about 1455, 1410, and 875 cm^{-1} ([Fleet and Liu, 2003](#)). The spectrum of the pterosaur bone exhibits bands at 1456, 1425, and 873 cm^{-1} , indicating that the CO_3^{2-} substitutes for the PO_4^{3-} groups (B-type). This B-type substitution reveals that the CO_3^{2-} in the environment replaced some of the PO_4^{3-} in the hydroxyapatite during the fossilization process.

In addition, the phosphate crystallinity index (PCI), which provides an estimation of the crystallinity of the pterosaur bones, can also be used to investigate the effects of diagenesis and fossilization on the lattice structure and composition of the bioapatite. The higher the PCI, the higher the degree of crystallinity ([Lai, 2006](#)). Generally speaking, the crystals in fresh bones have PCI values of 2.8–3.0, while diagenetic bones have much higher values ([Berna et al., 2004](#)). According to the calculation formula obtained from the literature ([Shemesh, 1990](#); [Weiner and Bar-Yosef, 1990](#)), the PCI value of the fossils is 4.17, indicating that a high degree of diagenetic alteration occurred during burial, and the fossil pterosaur bones have undergone severe diagenesis.

2.2.4 Bone histology

The sample was embedded in EXAKT Technovit 7200 one-component resin for the longitudinal section preparation, and then, it was cut with an EXAKT 300CP automatic micro-

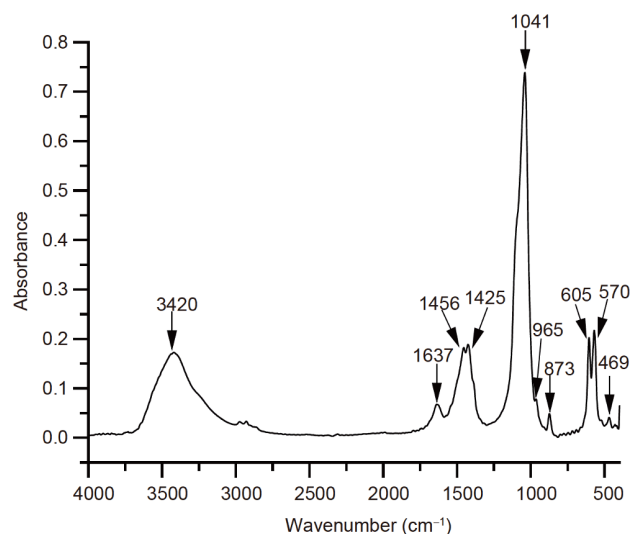


Figure 4 FTIR spectrum of a fossil bone.

tomic microtome. The section was prepared by grinding and polished it to about 30 μm using an EXAKT 400CP variable speed grinder-polisher and P500 and P4000 abrasive paper. The thin section was photographed in both plane-polarized light (PPL) and crossed polarized light (XPL) under a ZEISS Axio imager A2m polarized light microscope. The results are shown in [Figure 5](#).

The thin section reveals that the pterosaur bone has numerous vascular canals in a reticular pattern ([Figure 5a](#)). Furthermore, the black region may be caused by the invasion of bacteria. The line of arrested growth (LAG) and cracks can be observed at the cortical bone ([Figure 5e](#)). Under crossed-polarized light, many crystals, which are probably composed of calcite, can be observed in the canals ([Figures 5b and 5d](#)).

2.2.5 SEM-EDS

A rubber suction bulb was used to generate air to clean the samples. Then, the samples were secured in an instrument

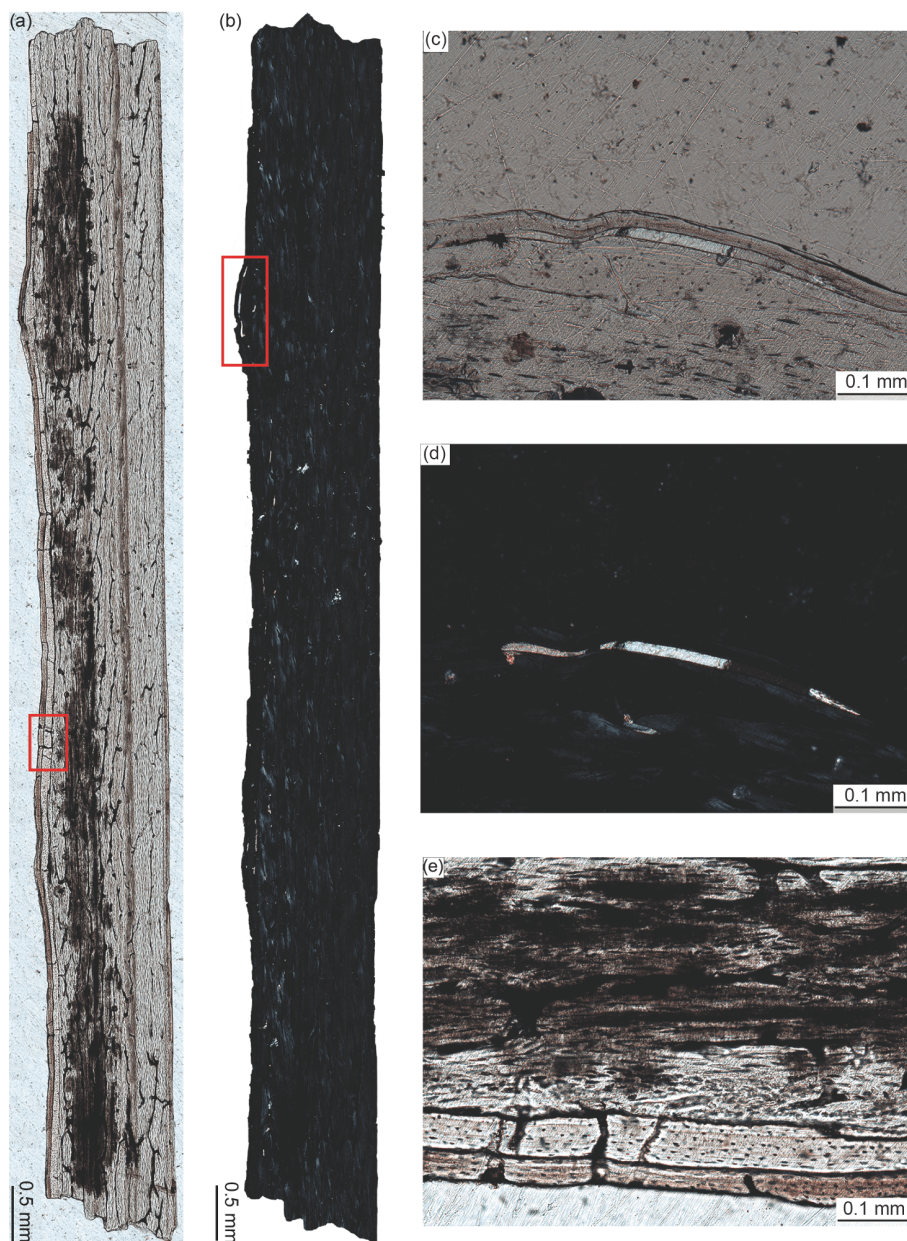


Figure 5 Microphotographs of the histological section. (a) Plane-polarized light, vascular canals in a reticular pattern and black spots on the surface. (b) Cross-polarized light, crystals can be observed in the canals. (c) Enlarged view of the red box in b, plane-polarized light. (d) Enlarged view of the red box in b, crystals can be observed in the canals under cross-polarized light. (e) Enlarged view of the red box in a, plane-polarized light. The LAG and cracks can be observed.

holder using conductive glue. The gold sputtered substrates were analyzed using a Carl Zeiss EVO25 (Zeiss, Germany) at 8–16 kV. The results are shown in Figure 6.

Cracks can be seen between the fossil bone and its filled matrix (Figure 6a), revealing that the broken bones easily spall under external forces. Although the bone surface shown in Figure 6b is relatively smooth and does not contain significant cracks, several cracks can be seen under high magnification (Figure 6c and 6d). These cracks will grow bigger under external forces. In addition, many crystals can also be observed in the thin section under high magnification (Figure 6e and 6f).

The Phenom-World Phenom XL at 15 kV was used to map the element distributions of the thin section. The composition of the darker areas in the vascular canals in the backscattered electron image were compared with those of the brighter regions using area-scanning analysis. The region shown in Figure 5d was also tested to determine its composition.

Under the backscatter electron detector (BSD) model, the region will be brighter as the atomic number increases. Figure 7a shows that some areas are much brighter, while others are not significantly different from the surrounding area, which indicates that there are different materials filling in the vascular spaces. The SEM-BSD image containing

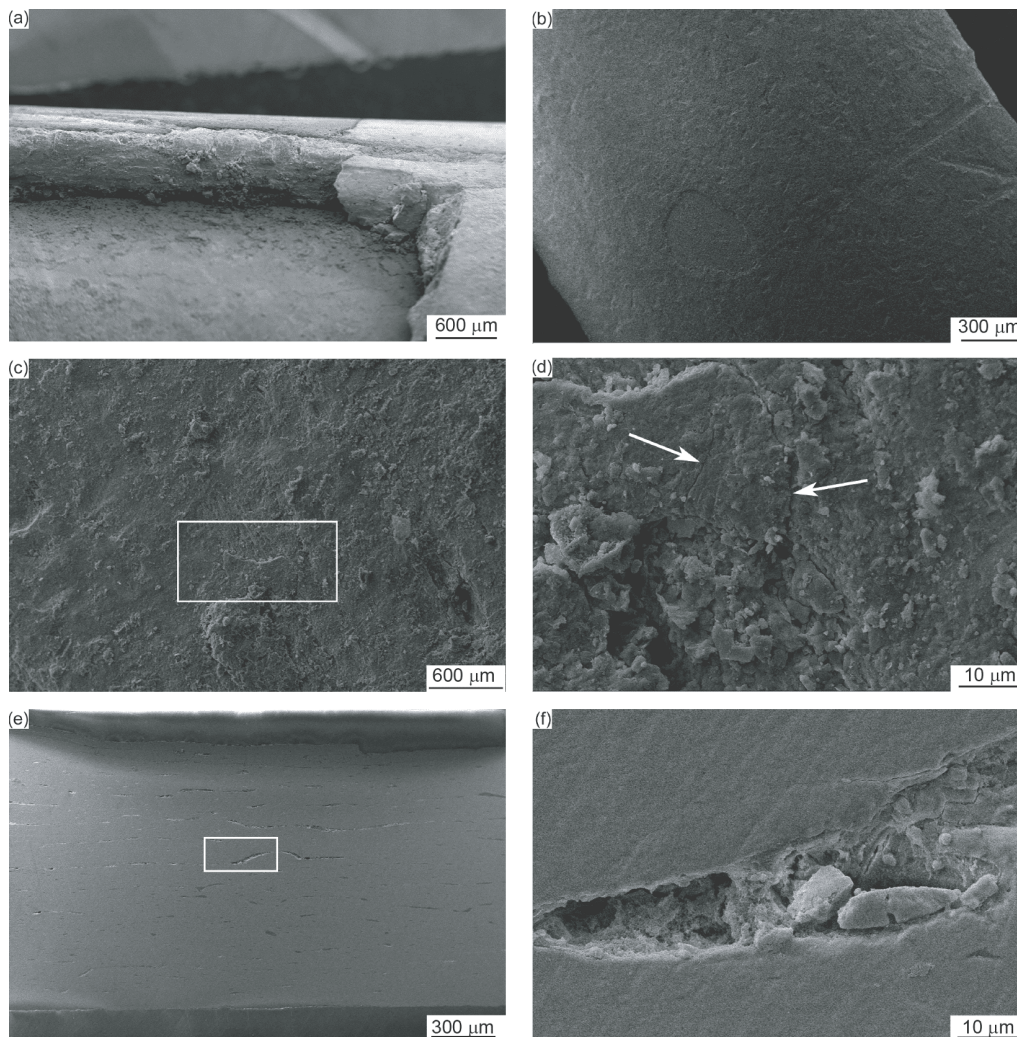


Figure 6 SEM images of the fossil bone and its thin section. (a) The fracture surface of the pterosaur bone. (b) Low magnification image of the bone's surface. (c) High magnification image of the bone's surface, containing small cracks. (d) Enlarged view of the white box in (c), cracks can be seen (white arrow). (e) Bone tissue slice (vertical axis). (f) Enlarged view of the white box in (e), crystals can be observed in the canals.

bright regions (Figure 7d) is rich in Mn, O, and F, but it contains almost no Ca and P, indicating that this area is composed of manganese cement. The SEM-BSD image containing dark regions within the vascular canals (Figure 7e) is rich in Ca and O, but contains almost no P and F, indicating that this area composed of calcite cement. The element detection results for the same region shown in Figure 5d indicate that the crystal is calcite, and this area has a very high Ca and O contents, but contains almost no P and F.

The calcite and manganese cements in the vascular canals should be the result of the mineral composition of the groundwater deposited in the bone cavity after the decay and disappearance of the organic matter during the long-term burial (Du and Tong, 2009). In the early stages of the burial process, CaCO_3 does not deposit easily because of acidic gases such as H_2S and CO_2 , which are generated during the organic decay, which can dissolve in water and reduced the pH value (Ronald, 1999). The deposition of CaCO_3 begins

only when the fleshy organic matter has rotted away and the pH of the microenvironment increases.

2.2.6 Ion chromatography

A Shimadzu (Kyoto, Japan) HIC-10A super IC system was used to analyze the contents of the soluble salts in the pterosaur fossils. The detailed experimental methods were the same as that reported by Li et al. (2019). The analytical conditions are reported in Table 3.

Table 4 shows that the contents of Na^+ , Cl^- , and NO_3^- are very high in the rocks surrounding the fossil bones, while the filler in the fossil bones has lower soluble salt contents. The high soluble salt contents within the fossil bones may be due to the fact that soluble salts, such as NaCl , begin to dissolve and migrate from the surrounding rocks into the fossil bones when the humidity changes. However, the ions may have difficulty migrating from the bones into fillers because hydroxyapatite has a good adsorption capacity (Shen et al.,

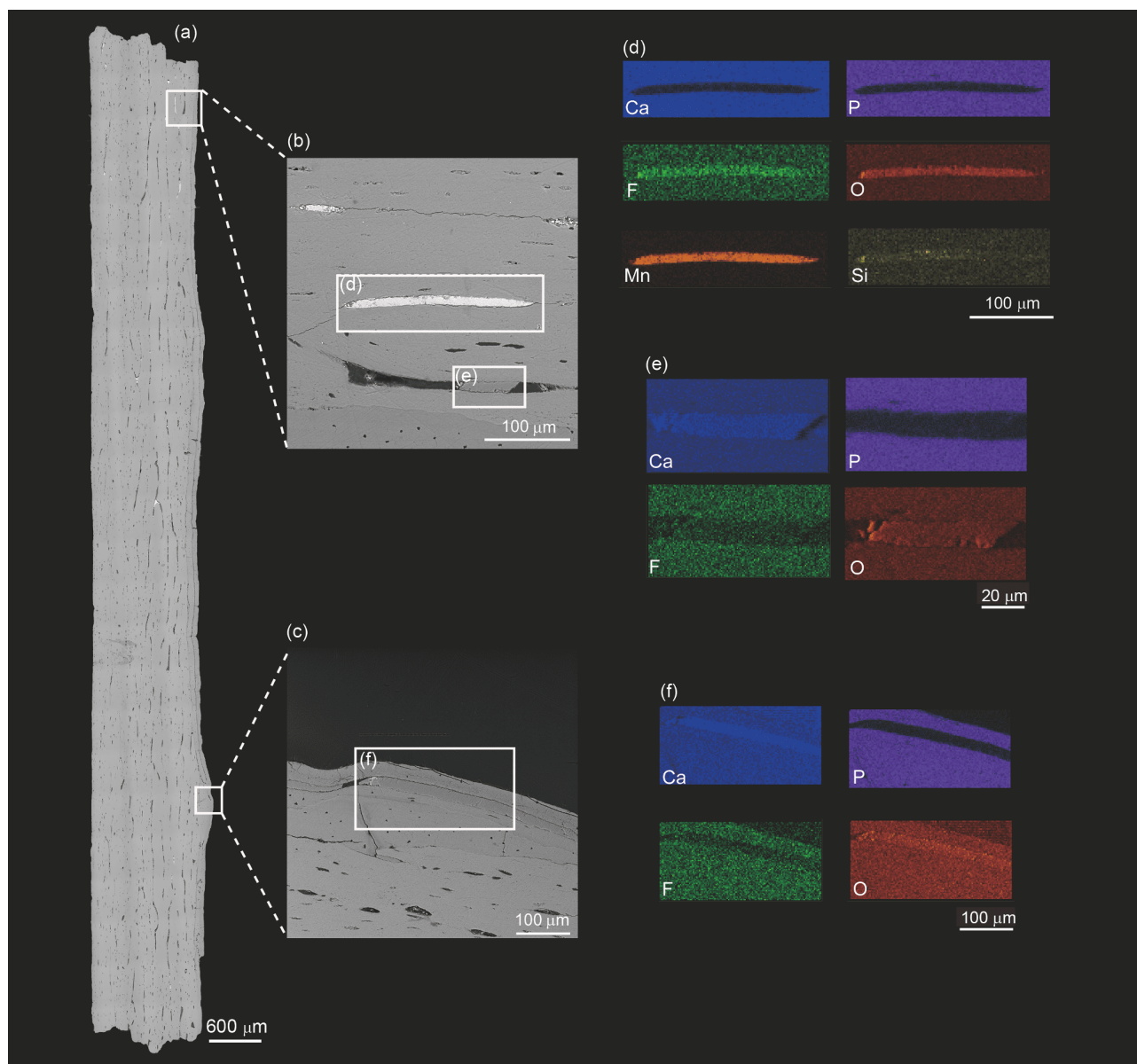


Figure 7 The surface scans and the elemental compositions of the bone thin section obtained from the SEM energy spectrum. (a) Image of the bone thin section under the BSD model. (b) Enlarged view of the white box in a, some crystals are light in color, while others are dark. (c) Enlarged view of the white box in a, the scanned area is the same part as in Figure 5c and 5d. (d) The elemental composition of the light area in (b), which is rich in Mn, O, and F and poor in Ca and P. (e) The elemental composition of the dark area in (b), which is rich in Ca and O and poor in P and F. (f) The elemental composition of the dark area in (c), which is rich in Ca and O and poor in P and F.

Table 3 The analytical conditions of the IC

Items	Cations	Anions
Mobile phase	0.70 mmol L ⁻¹ sulfuric acid	0.35 mmol L ⁻¹ sodium carbonate
Column temperature	40°C	45°C
Flow rate	1.0 mL min ⁻¹	0.8 mL min ⁻¹
Pressure	3.7 MPa	11 MPa
Injection volume	60 μL	60 μL
LC start time-stop time	0–30 min	0–20 min

1996). The adsorption capacity of the fossil bones explains why the salt contents of the bones are much higher than those

of the hollow bone fillers. Furthermore, the sulfate was formed in an aerobic environment during the decay and decomposition of the organic matter after the pterosaur was buried, which resulted in the fossil bones having a higher sulfate content than the matrix (Weiner, 2010). The specific reasons for the high sulfate contents of the fossil bones needs to be investigated further.

3. Discussion

Based on the above analysis results, we obtained important

Table 4 The soluble salt contents of the fossils ($\mu\text{g g}^{-1}$)

Sample	Na ⁺	K ⁺	Ca ²⁺	Mg ²⁺	Cl ⁻	NO ₃ ⁻	SO ₄ ²⁻	Total
F-Black	315.60	95.03	2688.89	0.00	197.12	378.45	2391.71	6066.80
F-White	152.46	129.01	1589.02	0.00	54.66	67.42	362.56	2355.13
F-Bone	3679.23	69.47	7837.83	0.00	10866.17	4185.44	8946.27	35584.41
F-Rocks	5478.11	150.60	4159.94	255.46	14958.99	4173.35	199.48	29375.93
F-Clay	7971.75	354.61	10621.40	1151.23	29263.74	14178.72	174.15	63715.59

details about pterosaur fossil bones and the matrix that fills them. The fossil bones are mainly composed of hydroxyapatite, but CO_3^{2-} was substituted for some of the PO_4^{3-} in the B site (i.e., carbonate hydroxyapatite). The PCI of the fossil bones was 4.17, which is much higher than that of unfossilized bones (2.8–3.0). This high PCI value reveals that fossils have experienced severe diagenesis (Berna et al., 2004). The vascular canals are filled with calcite and manganese cement, which also indicates that the bones have been fossilized. The main mineral components of the sandstone-filled matrix within the hollow bones are calcite, quartz, and feldspar. Moreover, the light-colored filling contains a small amount of dolomite and clay minerals compared with the dark-colored filling, and the dark-colored filling has a higher manganese content than the light-colored filling. Secondary precipitation products filling in the canals and cavities have been observed in many of the fossils (Monge et al., 2014). The reason for this phenomenon is that calcium carbonate-rich water evaporates and the calcite is deposited within the small cavities left by the organic decomposition. The phenomenon of secondary calcite filling indicates that the fossil has experienced alternating dry and wet environmental conditions (Monge et al., 2014). The manganese cement also fills in the small cavities. This is because when the pterosaurs were buried in sediments containing Mn-rich groundwater, the dissolved manganese was transported into the vascular spaces in the bones. The manganese was deposited in the bones when the solution evaporated (Pfretzschner and Tütken, 2011). It is generally believed that the presence of Mn oxides indicates that the fossils were deposited in an oxidizing environment (Monge et al., 2014). However, determining the exact manganese mineral phase required the use of other complementary techniques because the detection limits of XRD are about 5% in a multi-component system (Ressler et al., 2001). Therefore, the specific reasons for the presence of manganese in these fossils needs to be investigated further. Furthermore, whether or not microorganisms were involved in the diagenesis of the pterosaur fossils also requires further investigation. Based on the above analysis of the fossils, the main reasons for the cracking and spalling of the fossil bones are as follows.

The first reason is physical weathering. Specifically, the fossil cracking was caused by the large amount of thermal stress caused by the dramatic temperature changes in the

Gobi Desert and the differences in the thermal expansion coefficients (TEC) of the various components of the fossils. Taking the Taklimakan Desert as a reference, the daily maximum and minimum temperatures in summer are 55 and 20°C, respectively, and the daily maximum and minimum temperatures in winter are 5 and 20°C, respectively (Zhang, 2016). Under the influence of a dramatic temperature difference, a large amount of thermal stress can be generated due to the different TEC of the different materials of the pterosaur fossils. The thermal stress consists of two components. (1) The TECs of the fossil bones and the calcite within the vascular canals are different. For calcite, the linear thermal expansion coefficient α parallel to the *c*-axis is $26.5 \times 10^{-6} \text{ K}^{-1}$, while the α perpendicular to the *c*-axis is $5.6 \times 10^{-6} \text{ K}^{-1}$ (Wu et al., 2016). These values reveal the anisotropic property of calcite, which means that calcite expands in one direction and contracts in the other. For hydroxyapatite (HA), which is the main component of the fossil bones, the linear thermal expansion coefficient α is $13.9 \times 10^{-6} \text{ K}^{-1}$ (Miyazaki et al., 2009). The different TECs of the fossil bones and calcite result in different expansion volumes, which cause thermal stress when the temperature changes. This large amount of stress can lead to thermal cracking. (2) The TECs of the surrounding rocks, the fossil bones, and the filling matrix are also different. The surrounding rocks are sandstone, and their linear thermal expansion coefficient (α) is 5×10^{-6} – $19 \times 10^{-6} \text{ K}^{-1}$ (Zhang et al., 2014). The fossil bones are mainly composed of hydroxyapatite, and its α is $13.9 \times 10^{-6} \text{ K}^{-1}$ (Miyazaki et al., 2009). The main component of the filling matrix is calcite, which has an α_{max} of $26.5 \times 10^{-6} \text{ K}^{-1}$ and an α_{min} of $5.6 \times 10^{-6} \text{ K}^{-1}$ (Wu et al., 2016). The different TECs of these three parts causes large amounts of thermal stresses at the boundaries between the surrounding rocks and the bones and at the boundary between the bones and the filling matrix when the temperature changes. Under this large amount of thermal stress, the tensile strength of the fossil bones decreases sharply due to the loss of organic material, and the fossil bones crack and spall under long-term stress.

The second reason is chemical weathering, especially salt damage. In recent years, substantial progress has been made in improving our understanding of the mechanism by which soluble salts damage porous materials (Jin et al., 2017). First, the crystalline pressure produced by the soluble salts during

crystallization can significantly damage porous materials. For instance, the crystallization pressure of halite is 221.9 MPa (Winkler, 1975), and the crystallization pressure of thenardite is greater than 7 MPa (Jin et al., 2015). Second, the volumetric expansion of salts during hydration can also exert pressure on porous materials. For example, the hydration pressure exerted during the transition from thenardite to mirabilite is 48 MPa (Goudie, 1998). Third, the TECs of salt crystals are different from that of the porous material, so thermal expansion can also exert pressure on the porous material (Goudie, 1998). These studies indicate that the damage soluble salts cause to porous materials is significant. Table 4 shows that fossil bones contain various soluble salts (e.g., NaCl, Na₂SO₄, and CaCl₂). These soluble salts generate significant pressure during the dissolution and recrystallization process when the environmental conditions change, e.g., from the arid Hami Basin to humid Beijing. This pressure will cause bone cracking and spalling if the pressure is greater than the tensile strength of the fossil bones. In fact, the strength of the bones will decrease dramatically because of the hydrolysis of the collagen. The tensile strength of fresh bone is about 47–66 MPa, while the tensile strengths of poorly preserved archaeological bones and well preserved bones are 4 MPa and 38 MPa, respectively (Turner-Walker and Parry, 1995). As can be seen from these data, the pressure generated by the soluble salts is much larger than the tensile strength of the fossil bones, so the fossil bones crack and spall.

Owing to the damage to cultural relics caused by salts, conservation scientists have set a limiting safety value for soluble salts in cultural relics. There is no risk when the NO₃⁻ content of the cultural relics is less than 500 μg g⁻¹, but desalination is required when the NO₃⁻ content is greater than 1500 μg g⁻¹. For Cl⁻, the safety value is less than 300 μg g⁻¹, and desalination is required when the Cl⁻ content is greater than 1000 μg g⁻¹ (Ottosen et al., 2007). Thus, the soluble salt contents in the pterosaur fossils are much higher than the limiting safety contents, which means that desalination and other conservation treatments are required. However, the traditional poultice desalination may not be a good choice because pterosaur fossils are sensitive to water (Li et al., 2019). Using crystallization inhibitors is a promising method of mitigating salt damage because crystallization inhibitors can limit the crystallization of the salt by preventing nucleation and by reducing the growth rates of specific faces, which both slow down the fossil decay (Granneman et al., 2019).

Therefore, the fossil weathering mechanism can be summarized as shown in Figure 8. For one thing, given the large daily temperature difference in the Gobi area, the large thermal stresses caused by the differences in the TECs of the various components can significantly damage pterosaur fossils. Similar thermal cracking occurred in dinosaur fossils

found in Zhucheng, Shandong, China. Researchers found that when the dinosaur fossils were preserved in an open container in direct sunlight, they were severely weathered; whereas when the fossils were displayed indoors and were coated with epoxy resin, they were only slightly weathered (Liu et al., 2019). This difference may be because thermal stress causes fossil cracking due to the heterogeneous recycling of sunlight and heat (Du et al., 2015; Zhang et al., 2018). These studies revealed that thermal stress is an essential factor leading to fossil weathering. For another thing, significant stress is generated by salt crystallization and hydration when the temperature and humidity change. This stress will cause the pterosaur fossils to crack when the pressure exceeds the tensile strength of the fossil bones. In addition to pterosaur fossil weathering, salt weathering is also a significant reason for the deterioration of other cultural relics, such as pottery (Zhao et al., 2015b), stone (Zhao et al., 2015a; Ji et al., 2020), and concrete (Teng, 2001; Wang et al., 2013).

Based on our research results, we conclude that the preservation conditions are vital for pterosaur fossils. Pterosaur fossils should be preserved in a constant temperature and humidity environment to avoid thermal cracking, and they should be consolidated to improve their strength. Because the fossils are water-sensitive, using a poultice may not be a good method (Li et al., 2019), and using crystallization inhibitors such as potassium ferrocyanide may be more effective. Since saline soil is distributed widely in China (Zhang and Kuang, 1990), fossils excavated from similar conditions may also suffer salt weathering. Thus, we suggest that fossils excavated from high saline sites should be placed in a constant temperature environment to avoid the damage caused by the salt dissolution and recrystallization. In addition to this, IC analysis is recommended because it can be used to determine whether soluble salts are a deterioration factor or not, and this information can help the conservator develop an effective preservation plan.

Overall, this is the first study that has focused on the weathering mechanism of vertebrate fossils in Xinjiang, and the results provide insights into the preservation and conservation of fossil bones from extremely arid and highly saline areas and for fossils from similar environments around the world.

4. Conclusions

The study aimed to determine the weathering mechanism of pterosaur fossils. The findings of this study are as follows.

(1) The main component of the fossil pterosaur bones was hydroxyapatite, and carbonate substituted for some of the phosphate. Calcite and manganese oxides were precipitated in the vascular canals. The main mineral within the hollow

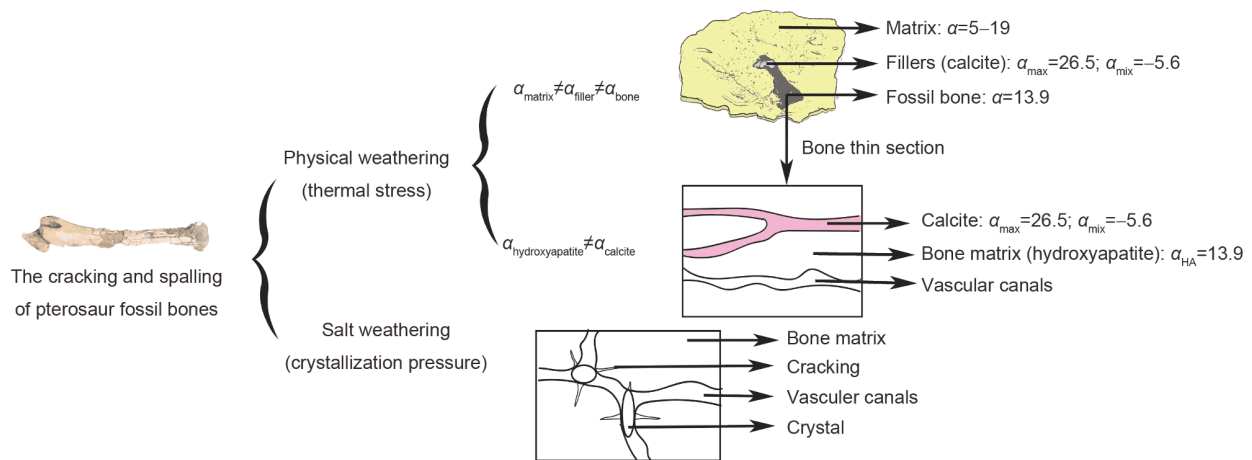


Figure 8 (Color online) Schematic diagram of pterosaur fossil weathering. α is the coefficient of thermal expansion (10^{-6} K^{-1}); HA is hydroxyapatite. Because the composition of the sandstone-filled matrix is complex and calcite is the main component of the filler matrix (over 45%), the calcite TEC was used as a reference for the TEC of the filler.

bones was calcite, with some feldspar and quartz. The fossil bones contained a large number of anions and cations such as Cl^- , NO_3^- , SO_4^{2-} , Na^+ , and Ca^{2+} .

(2) One crucial reason for the cracking of pterosaur bones is the enormous thermal stress caused by the dramatic temperature changes in the Gobi Desert and the differences in the TEC of different materials.

(3) Another reason for the pterosaur fossils weathering is the large stress generated by salt crystallization when the temperature and humidity change. Pterosaur fossils will be damaged when the crystallization pressure exceeds the tensile strength of the fossils.

(4) Crystallization inhibitors, such as potassium ferrocyanide, can be applied to avoid weathering damage caused by the repeated dissolution and recrystallization of soluble salts. In addition, organosilicone and other materials can be used to consolidate the fossils and to improve their strength. The weathering mechanisms discussed and the conservation procedures suggested in this article are very important for the preservation and conservation of fossil bones from extremely arid and highly saline areas.

Acknowledgements We are grateful to Hongjiao Zhou, Long Xiang, Xun Jin, Yang Li, He Chen, Xinjun Zhang, Junxia Wang, Xiaodi Liu, Shiwei Song, Xufeng Zhu, Yue Chen, Jing Du, Fengdan Hu, Jianfeng Cui, Xueqi Zhou and Chenyang Jiangxiao for the help in the fieldwork and laboratory tests. We also thank the reviewers for providing valuable comments. This work was supported by the National Natural Science Foundation of China (Grant Nos. 41572020 & 41688103), the Youth Innovation Promotion Association of CAS (Grant No. 2019075) and the Foundation of Excavation and Protection from the Hami Government.

References

Berna F, Matthews A, Weiner S. 2004. Solubilities of bone mineral from archaeological sites: The recrystallization window. *J Archaeol Sci*, 31: 867–882

- Deeming D C. 2017. How pterosaurs bred. *Science*, 358: 1124–1125
- Deng J G, Liu D L, Ye Y. 2010a. Protecting materials of dinosaur fossils (in Chinese). *J Henan Normal Univ-Nat Sci*, 38: 156–159
- Deng J G, Peng G Z, Jin Y Z, Ye Y. 2010b. Study on the characterization of dinosaur fossils and their surrounding rocks from Zigong (in Chinese). *Chin J Spectrosc Lab*, 27: 192–196
- Du S X, Zhang S K, Yu X F, Chen J, Song X S, Jia C, Zhang G R. 2015. Analysis and study on TM coupling method to weathering effect of dinosaur fossil (in Chinese). *Shandong Land Resour*, 31: 65–70
- Du Y S, Tong J N. 2009. Introduction to the History of Paleontology (in Chinese). Wuhan: China University of Geosciences Press. 6
- Fleet M E, Liu X. 2003. Carbonate apatite type A synthesized at high pressure: New space group and orientation of channel carbonate ion. *J Solid State Chem*, 174: 412–417
- Goudie A. 1998. The salt weathering hazard in deserts. In: Kalvoda J, Rosenfeld C L, eds. *Geomorphological Hazards in High Mountain Areas*. Dordrecht: Springer. 107–120
- Granneman S J C, Lubelli B, van Hees R P J. 2019. Mitigating salt damage in building materials by the use of crystallization modifiers—A review and outlook. *J Cultural Heritage*, 40: 183–194
- Hackett C J. 1981. Microscopical focal destruction (tunnels) in exhumed human bones. *Med Sci Law*, 21: 243–265
- Howie F M P. 1984. Materials used for conserving fossil specimens since 1930: A review. *Stud Conserv*, 29: 92–97
- Ji J, Wang Y J, Ma T, Wang Z, Dong S H, Zhou W Q. 2020. Analytical study of contaminants and soluble salts on the surface of stone sculptures at Mao Mausoleum, Shaanxi (in Chinese). *Sci Conserv Archaeol*, 32: 22–28
- Jin Z L, Chen G Q, Xia Y, Su B M, Zhou T, Lv G X. 2015. Comparative study of salt damage caused by sulfates and chlorides to mural paintings—Evidence of superpenetration, migration and crystallization destruction resulting from sodium sulfate (in Chinese). *Sci Conserv and Archaeol*, 27: 29–38
- Jin Z L, Liu D D, Zhang Y K, Chen G Q, Xia Y, Su B M, Zhou T, Lv G X, Luo H J. 2017. Salt migrations and damage mechanism in cultural heritage objects (in Chinese). *Sci Conserv Archaeol*, 29: 102–116
- Lai C. 2006. Study on the synthesis of hydroxyapatite nanowires with reverse micellae-solvothermal method and its mechanism (in Chinese). Doctoral Dissertation. Changsha: Hunan University. 31
- Li Y, Luo W G, Yang Y M, Wang X L. 2019. The weathering mechanism of surrounding rocks in Hamipterus fossil (in Chinese). *Acta Palaeontol Sin*, 58: 515–525
- Liang T. 2009. Preliminary analysis for the diseases of earthen sites in Xinjiang (in Chinese). *Archaeol Cult Relics*: 103–106

- Liu F C, Zhang S K, Tian J X, Jia C, Chen J, Chen W F. 2019. Simulated study on the effects of direct sunlight, indoor shading and protective layers on the weathering of dinosaur fossils (in Chinese). *Shandong Land Resour*, 35: 58–61
- Liu L X. 2014. Study on mechanism and consolidation of ivory fossil in Chengcheng County (in Chinese). *Archaeol Cult Relics*: 100–103
- López-Polín L. 2012. Possible interferences of some conservation treatments with subsequent studies on fossil bones: A conservator's overview. *Quat Int*, 275: 120–127
- López-Polín L, Ollé A, Cáceres I, Carbonell E, Bermúdez de Castro J M. 2008. Pleistocene human remains and conservation treatments: The case of a mandible from Atapuerca (Spain). *J Human Evol*, 54: 539–545
- Mallouchou M S, Stathopoulou E T, Theodorou G E. 2019. How do fossilized mammalian bones behave during chemical conservation? The histological case studies of Tilos and Kerassia. *Geoheritage*, 11: 597–614
- Martill D M. 2014. Palaeontology: Which came first, the pterosaur or the egg? *Curr Biol*, 24: R615–R617
- Miyazaki H, Ushiroda I, Itomura D, Hirashita T, Adachi N, Ota T. 2009. Thermal expansion of hydroxyapatite between -100°C and 50°C . *Mater Sci Eng-C*, 29: 1463–1466
- Monge G, Carretero M I, Pozo M, Barroso C. 2014. Mineralogical changes in fossil bone from Cueva del Angel, Spain: Archaeological implications and occurrence of whitlockite. *J Archaeol Sci*, 46: 6–15
- Newesely H. 1989. Fossil bone apatite. *Appl Geochem*, 4: 233–245
- Ottosen L M, Pedersen A J, Rørig-Dalgaard I. 2007. Salt-related problems in brick masonry and electrokinetic removal of salts. *J Build Apprais*, 3: 181–194
- Peng X, Wang Y, Ma X F, Bao H, Huang X, Zhou H, Luo H, Wang X. 2020. Sol-Gel derived hybrid materials for conservation of fossils. *J Sol-Gel Sci Technol*, 94: 347–355
- Pfretzschner H U, Tütken T. 2011. Rolling bones—Taphonomy of Jurassic dinosaur bones inferred from diagenetic microcracks and mineral infillings. *Palaeogeogr Palaeoclimatol Palaeoecol*, 310: 117–123
- Ressler T, Wienold J, Jentoft R E. 2001. Formation of bronzes during temperature-programmed reduction of MoO_3 with hydrogen—An *in situ* XRD and XAFS study. *Solid State Ion*, 141–142: 243–251
- Ronald E M. 1999. Taphonomy: A Process Approach. Cambridge Cambridge University Press
- Shemesh A. 1990. Crystallinity and diagenesis of sedimentary apatites. *Geochim Cosmochim Acta*, 54: 2433–2438
- Shen W, Gu Y F, Liu C S, Sun X M, Hu L M. 1996. Surface characteristics of hydroxyapatite (in Chinese). *B Chin Ceram Soc*, 45–52
- Teng X M. 2001. Conservations about salt damage control of concrete Bridges along the sea of Japan (in Chinese). *World Bridges*, 57–63
- Turner-Walker G, Parry T V. 1995. The tensile strength of archaeological bone. *J Archaeol Sci*, 22: 185–191
- Turner-Walker G. 1998. The West Runton fossil elephant: A pre-conservation evaluation of its condition, chemistry and burial environment. *Conservator*, 22: 26–35
- Turner-Walker G. 2012. Early bioerosion in skeletal tissues: Persistence through deep time. *Neues Jahrb Geol Palaontol Abh*, 265: 165–183
- Wang J, Chen J J, Ju Z Q. 2013. Research on the mechanism and types of shaft lining reinforced concrete corrosion in salt disasters environment (in Chinese). *Sci Techno Eng*, 13: 1690–1694
- Wang L, Fan H, Liu J, Dan H, Ye Q, Deng M. 2007. Infrared spectroscopic study of modern and ancient ivory from sites at Jinsha and Sanxingdui, China. *Mineral Mag*, 71: 509–518
- Wang X L, Jiang S X, Chen X. 2018. Study on Hamipterus and their 3D embryos (in Chinese). *Sci Technol Rev*, 36: 11–19
- Wang X, Kellner A W A, Jiang S, Cheng X, Wang Q, Ma Y, Paidoula Y, Rodrigues T, Chen H, Sayão J M, Li N, Zhang J, Bantim R A M, Meng X, Zhang X, Qiu R, Zhou Z. 2017. Egg accumulation with 3D embryos provides insight into the life history of a pterosaur. *Science*, 358: 1197–1201
- Wang X, Kellner A W A, Jiang S, Wang Q, Ma Y, Paidoula Y, Cheng X, Rodrigues T, Meng X, Zhang J, Li N, Zhou Z. 2014. Sexually dimorphic tridimensionally preserved pterosaurs and their eggs from China. *Curr Biol*, 24: 1323–1330
- Weiner S, Bar-Yosef O. 1990. States of preservation of bones from prehistoric sites in the Near East: A survey. *J Archaeol Sci*, 17: 187–196
- Weiner S. 2010. Microarchaeology: Beyond the Visible Archaeological Record. New York: Cambridge University Press. 59
- Weng S F, Xu Y Z. 2016. Fourier Transform Infrared Spectroscopy. 3rd ed. Beijing: Chemical Industry Press
- Winkler E M. 1975. Stone: Properties, Durability in Man's Environment. 2nd ed. New York: Springer-Verlag Wien GmH. 121
- Wu F Q, Wu W D, Su F F, Shi M. 2016. Temperature characteristics of optical calcite crystals (in Chinese). *Acta Opt Sin*, 36: 267–272
- Zhang S K, Yu X F, Jia C, Du S X, Song X S, Chen C, Liu F C, Chen J, Chen W F. 2018. Effect study on thermal stress to weathering damage of dinosaur fossils (in Chinese). *Shandong Land Resour*, 34: 42–48
- Zhang S K, Yu X F, Jia C, Du S X, Song X S, Liu F C, Chen J, Chen W F. 2019. Study on main factors affecting weathering damage to dinosaur fossils and surrounding rocks and weathering mechanism (in Chinese). *Shandong Land Resour*, 35: 25–31
- Zhang W B. 2016. Variation of soil heat flux in the Taklamakan Desert (in Chinese). Dissertation for Master's Degree. Xinjiang: Xinjiang Normal University. 30
- Zhang X H, Yang Y, Yu Y Y. 2014. Material Manual 6 (in Chinese). Harbin: Harbin Institute of Technology Press
- Zhang C Y, Kuang X F. 1990. The determination of soluble salts and water mineralization of soil in Xinjiang by ion chromatograph (in Chinese). *Arid Zone Res*, 63–72
- Zhao G T, Li Y H, Zhang Y D, Du D X. 2015a. Analysis of the factors in masonry surface weathering of Ming Dynasty City Wall in Xi'an (in Chinese). *J Shaanxi Normal Univ-Nat Sci Ed*, 43: 54–58
- Zhao J, Wang L Q, Luo H J, Li W D, Rong B, Zhou T. 2015b. The effects of the soluble salts NaCl and CaCl_2 on pottery efflorescence (in Chinese). *Sci Conserv Archaeol*, 27: 1–6

(Responsible editor: Min ZHU)